Characterizing the spatial non-uniformity and temporal stability of QWIP and T2SL cooled infrared detector focal plane arrays

Waldo van der Westhuisen[1], *Mathews* Chirindo[1*] and *Josiah* Jideani[1]
[1]Council for Scientific and Industrial Research, Manufacturing Cluster, South Africa

Abstract. Fixed pattern and temporal noise in infrared Focal Plane Arrays are inherent in the technology and must be corrected to achieve optimal performance in optical gas imaging. These noise sources are intrinsic to the manufacturing process of these devices and the read-out electronics. This paper presents the characteristics of these noise sources for Type 2 Superlattice and Quantum Well Infrared Photodetectors. Experimental results visualise the raw uncorrected non-uniformity of the respective focal plane arrays along with their gain and offset correction tables. The Quantum Well Infrared Photodetector (Sulphur Hexafluoride) shows better uniformity in the uncorrected frames than the Type 2 Superlattice (Volatile Organic Compound), but both detectors show similar performance after correction. The corrected frames are evaluated and a quantity, the absolute median residual per frame, is presented to quantify the residual non-uniformity after correction. Results show that the standard 2-point NUC is effective at correcting the non-uniformity with low levels of remaining noise.

1 Introduction

Advanced cooled infrared Focal Plane Array (FPA) technologies such as Type 2 Superlattice (T2SL) and Quantum Well Infrared Photodetectors (QWIP) have shown great potential and success in enabling infrared imaging technologies, such as Optical Gas Imaging (OGI) [1]. However, in operating these FPAs and achieving the required performance, there are non-ideal spatial and temporal noise sources to be considered [2].

Spatial non-uniformity refers to the variation in pixel-to-pixel response when uniformly illuminated. This source of noise is spatially consistent and can be referred to as fixed pattern noise and can be corrected for* using a standard 2-point Non-Uniformity Correction (NUC) algorithm [1-3]. Temporal noise manifests as varying pixel values between successive frames over time and represents a statistical distribution around a mean or median value. This source of noise cannot be eliminated entirely using a 2-point NUC.

Many approaches are presented in literature to propose different strategies for NUC with a goal to improve non-uniformity in infrared detectors. In some cases, NUC is scene-based [4, 3, 5]. In this case the infrared camera is calibrated for the scene and hence must provide optimal performance. The techniques reported vary from adaptive background modelling

* Corresponding author: mchirindo@csir.co.za

where the drift of the detectors is based on a single Gaussian distribution [4] to field upgradability further to normal black body calibration [4, 5]. In both scenarios, the update of the parameters is selectively performed based on the scene.

In most cases though, NUC calibration is performed in the laboratory [6-10] where the computed gain and offset maps are stored in the camera's non-volatile memory for use in the field. This works well, especially for temperatures within the range of calibrated points. Laboratory NUC calibrations often provide room for computing gain and offset maps from multiple frames since data storage is not a constraint. Computing gain and offset maps from multiple frames is also known to reduce the effect of temporal variation on a per pixel basis.

Other works which can be laboratory based and/or scene based rely on a single frame NUC calibrations [6, 7, 11]. This is particularly relevant where storage requirement is a constraint while operating in real time is desirable.

However, although all these works outlined above come with their varying degrees of performance in correcting the non-uniformity in infrared images, none of them provide an objective analysis necessary to characterize the spatial non-uniformity and temporal stability of specific FPA technologies. Such characterization, if performed have the potential to provide guidance into specific NUC strategies required to obtain optimal performance of the optical imaging devices. This work focusses on analysing raw and corrected image frames to provide characteristics of the spatial and temporal noise for QWIP and T2SL detectors. An evaluation of the residual non-uniformity after a correction algorithm is applied will be presented.

The rest of the paper is organised as follows: Section 2 briefly outlines the methodology employed to perform the characterization of spatial non-uniformity and temporal stability for QWIP and T2SL detectors. Section 3 provides the experimental conditions while section 4 presents the experimental results for the detector characteristics. Section 5 concludes the paper and projects some future work.

2 Methodology

In evaluating the QWIP and T2SL detectors, a laboratory setup was used to capture data from the cameras under test using a PCIe based image acquisition card (PCIe-7360) that communicated with MATLAB. The detector was directed at a full field black body that uniformly illuminated the FPAs. 100 raw frames were then acquired for each integration time between 1ms and 16ms in steps of 1ms. Two different reference temperatures were used for each camera as required by the NUC correction algorithm. Further processing and analysis to characterize the raw image and processed frames was performed in the MATLAB environment. A 2-point NUC correction algorithm is applied, and an evaluation of the residual noise will be presented.

2.1 Spatial non-uniformity

To qualitatively evaluate the spatial non uniformity in the raw images of the QWIP and T2SL FPAs, a one- and two-dimensional approach was taken. Firstly, to evaluate the horizontal and vertical non-uniformities separately, the 100-frame data per integration time was processed to create a single frame where each pixel corresponds to the temporal median value across the 100 frames. The temporal median $M(x.y)$ of each pixel at position (x, y) over 100 frames $(F_1, F_2 \dots \dots \dots F_{100})$ is given by:

$$M(x.y) = median(F_1(x,y), F_2(x,y), \dots \dots \dots \dots F_{100}(x,y)) \quad (1)$$

This operation is applied independently to each pixel for all $x = 0\ to\ 319$ (image width) and for all $y = 0\ to\ 255$ (image height) to form a frame of medians.

This frame, for each integration time, was then further processed to select the median pixel value for each column or row. Thus, the median value, $C(x)$ for each column and, $R(y)$ for each row is represented by:

$$C(x) = median(M(x,0), M(x,1), M(x,2), \dots, M(x,255)) \quad (2)$$

$$R(y) = median(M(0,y), M(1,y), M(2,y), \dots, M(319,y)) \quad (3)$$

This resulted in a 1-dimensional plot representing the horizontal and vertical variations in pixel intensities. All integration times are plotted together to show the evolution of the non-uniformities with an increase in integration time

Secondly, to evaluate the two-dimensional distribution of spatial non-uniformities for each integration time, the temporal median frame generated from the 100-frame stack was plotted on a surface heat map. Once again, the output was used to qualitatively evaluate the spatial non-uniformities and to evaluate the evolution thereof with an increase in integration time

Lastly, histograms of the median frames were plotted to show the distribution of the pixel values in the temporal median frames for each integration time.

2.2 Temporal non-uniformity

Similar to the qualitative evaluation of spatial non-uniformity, the temporal variability of pixel response was investigated. To evaluate the temporal variability of pixels response the raw 100 frame stack at each integration time was processed and the values of 5 representative pixels were plotted together. For each pixel the standard deviation, s was calculated according to (4) and displayed in the legend.

$$s = \sqrt{\frac{1}{n-1}\sum_{i=1}^{n}(x_i - \tilde{x})^2} \quad (4)$$

where:

x_i is the pixel value for each ith frame.

$\tilde{x}$ is the mean (or median) for each pixel in all the frames.

n is the number of frames considered for temporal variability.

Next, for each integration time, the spatial distribution of pixel temporal variation was plotted on a surface heat map to evaluate if there is spatial consistency in the distribution of strongly varying pixels. Finally, to evaluate the statistical distribution of pixel values over time, a histogram was generated for 5 representative pixels and their values over the raw 100 frame stack were plotted together.

2.3 Gain and offset map generation

To generate the gain and offset maps, the camera manufacturer recommendations were followed in using a standard 2-point NUC. In doing so, the raw 100 frame stacks were considered, and, for each integration time, a high and low temperature stack was used as input to the NUC map generation. Prior to calculating the gain and offset maps, the high and low temperature input data stacks were processed to create single temporal median reference

frames where the temporal median for each pixel was found. Thereafter a spatial frame median for each single frame, for high and low temperature scenes, were found.

The gain and offset maps were then calculated using the following formulae[12, 13] and the resulting gain, G and offset, O maps were stored for later use.

$$G = \frac{median(S_{high}) - median(S_{low})}{S_{high} - S_{low}} \quad (5)$$

$$O = median(S_{low}) - G * S_{low} \quad (6)$$

where:
(S_{high}) is the pixel wise temporal median of the high temperature reference frame.
(S_{low}) is the pixel wise temporal median of the low temperature reference frame.
$median(S)$ is the median of the reference frame.

In qualitatively evaluating the gain and offset maps, surface heat maps were generated and compared over integration times.

2.4 Residual non uniformity evaluation

In evaluating the effectivity of the NUC correction algorithm, the residual non-uniformity of NUC corrected frames were evaluated. In doing so, the raw frames, used to generate the pixel wise median reference frame (S) and the frame median of the reference frame $median(S)$), were corrected with the gain and offset maps using the formula [12, 13].

$$F_{corrected} = G * F_{raw} + O \quad (7)$$

where:
$F_{corrected}$ is the corrected frame data
F_{raw} is the raw frame data

The resulting NUC corrected frames were then compared to the frame median, $median(S)$, and the pixel wise difference was found. The result of this step produced positive and negative differences, but the sign of the difference was not relevant in this evaluation, therefore the absolute values were considered. Finally, the median of the difference in the frame of residuals for each integration time was calculated. The resulting value for each integration time was then used as a measure of residual non uniformity and tables were generated to present the results for both high and low temperature scenes at integration times between 1ms and 16ms.

In qualitatively evaluating the residual non-uniformity, a surface heat maps were generated to visualize the spatial distribution of non-uniformities.

Finally, to evaluate the statistical distribution of pixel values over time, a histogram was generated for median absolute residual non uniformity at different integration times.

3 Experimental conditions

The experimental conditions under which measurements were taken for the two detector types are summarized in Table 1.

Table 1. Experimental conditions for the two camera (detector) types.

Camera type	Filter type	Band	Integration time (ms)	Low Temperature	High Temperature	Resolution
QWIP	SF6	Long wave IR	1ms to 16ms	18 °C	50 °C	320x256
T2SL	VOC	Medium wave IR	1ms to 16ms	15 °C	50 °C	320x256

4 Experimental results

The experimental results for the spatial and temporal non-uniformity, gain and offset maps as well as residual non-uniformity of the both the VOC and the SF6 detectors are presented in the following sub-sections.

4.1 Spatial non-uniformity VOC

This sub-section presents several spatial analysis visualizations of the median of raw frames created from 100 raw images for each integration time when viewing the high temperature full field black body at 50°C.

4.1.1 Temporal median frame, median row/column plots

In Fig. 1(a), the column-wise median pixel values of the VOC detector across all integration times are shown. Each curve represents the median along columns of the frame, highlighting horizontal fixed-pattern noise.

In Fig. 1(b), the row-wise median pixel values of the VOC detector across all integration times are shown. Vertical fixed-pattern noise and systematic shifts between rows are observable.

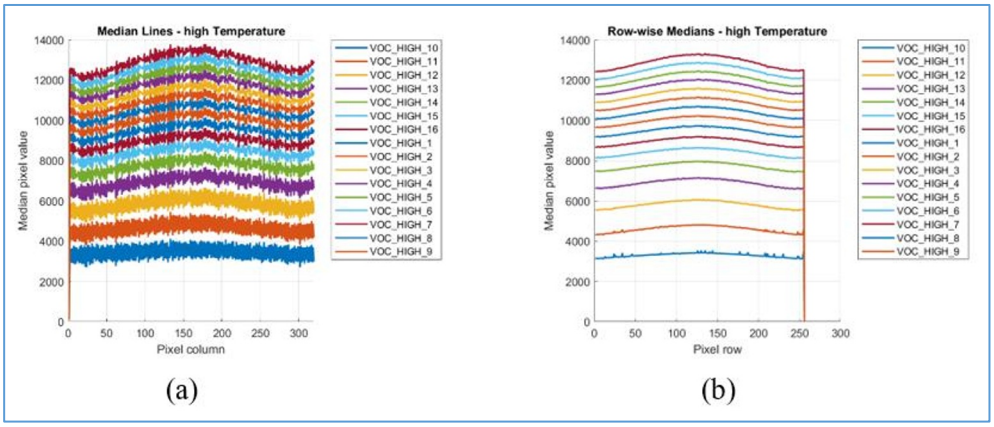

Fig. 1. (a) Column-wise median pixel values and (b) row-wise median pixel values.

4.1.2 Temporal median frame Heatmaps

In Fig. 2(a)-(c) the 2D surface plots of median frames for 1ms ,8ms and 16ms integration time are shown. These illustrate spatial non-uniformity patterns across the array before correction.

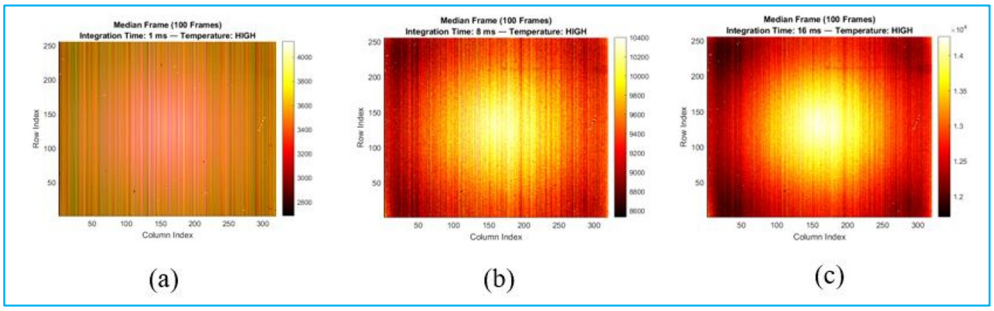

Fig. 2. Median frames for (a) 1ms, (b) 8ms and (c) 16ms.

4.1.3 Temporal median frame histograms

In Fig. 3(a)-(b) histograms of pixel values of median frames (VOC) across three integration times are shown. Bimodal distributions at low integration times indicate greater noise and non-uniformity.

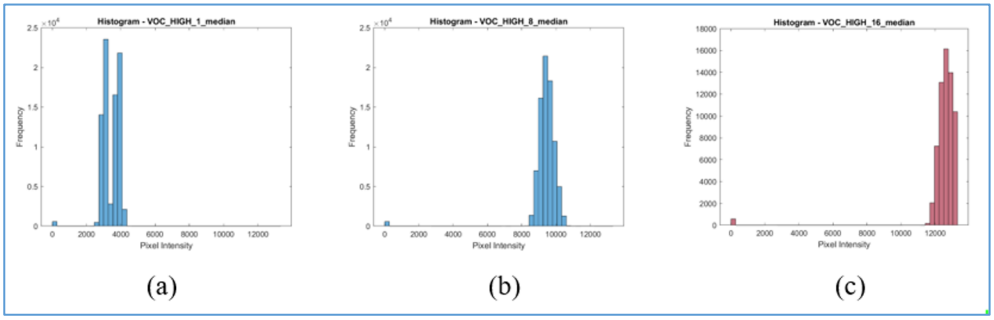

Fig. 3. Median frame for (a) 1ms, (b) 8ms and (c) 16ms integration times.

4.1.4 Discussion – spatial non-uniformity VOC

In the 1D column-wise and row-wise medians (Fig. 1), vertical or horizontal structures indicate column or row offsets in responsivity with the column-wise medians showing the most pronounced column to column variability. The 2D surface plots of the median frame (Fig. 2) further reinforce these findings, showing structured regions of higher and lower intensity. These patterns suggest both global gradients and localized pixel-to-pixel variation, consistent with residual non-uniformities typical of uncorrected sensors. The histograms of the median frame pixel values (Fig. 3) across integration times exhibit skewness and multimodality at certain integration times (ITs), hinting at local gain/offset issues.

Overall, spatial fixed-pattern noise is most prominent at shorter integration times, where signal-to-noise ratio (SNR) is lower.

4.2 Spatial non-uniformity SF6

This sub-section presents several spatial analysis visualizations of the median raw frames (100 raw images) for each integration time when viewing the high temperature full field black body at 50°C.

4.2.1 Temporal median frame, median row/column plots

In Fig. 4(a) the column-wise median pixel values for the SF6 detector across all integration times are shown. Smooth trends suggest less prominent horizontal fixed-pattern noise.

In Fig. 4(b) the row-wise median pixel values for the SF6 detector are shown. Minimal vertical artifacts indicate good spatial uniformity.

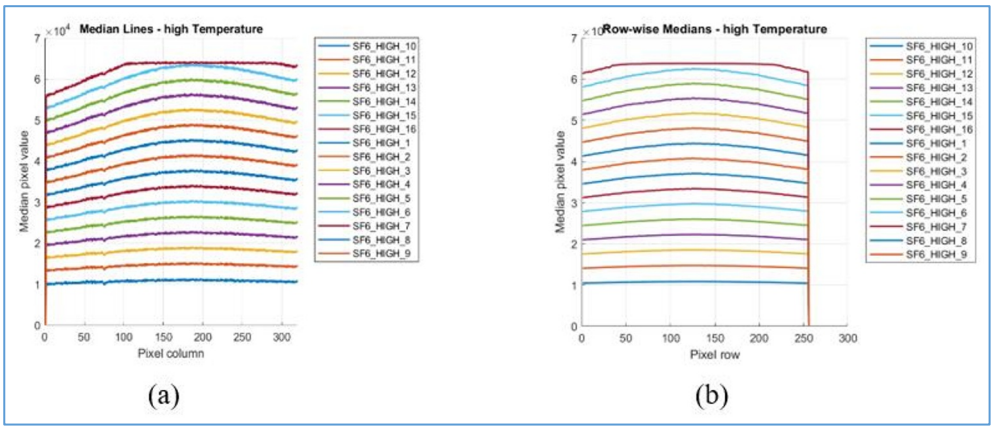

Fig. 4. (a) Column-wise and (b) row-wise median pixel values.

4.2.2 Temporal median frame heatmaps

In Fig. 5(a)-(c) the 2D surface plots of SF6 median frames are shown, visualizing spatial uniformity and any fixed-pattern structure of the FPA.

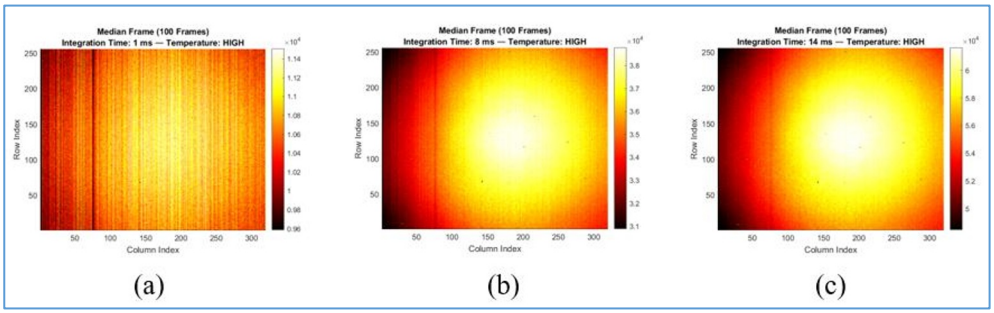

Fig. 5. Median frames for (a) 1ms, (b) 8ms and (c) 16ms integration times.

4.2.3 Temporal median frame histograms

In Fig. 6(a)-(c) histograms of pixel values from SF6 median frames across three integration times are shown. Narrower distributions suggest more consistent pixel response.

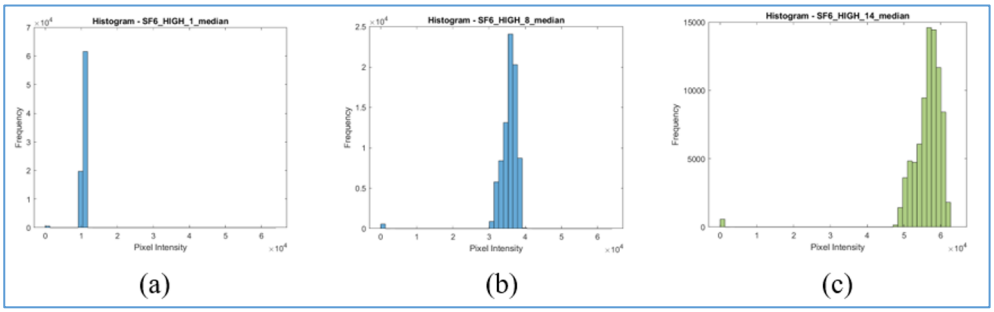

Fig. 6 Median frames for (a) 1ms, (b) 8ms and (c) 16ms integration times.

4.2.4 Discussion – spatial non-uniformity SF6

The spatial characteristics of the SF6 detector's median frames (Fig. 4 - Fig. 6) display a different pattern than the VOC camera. The SF6 FPA appears to exhibit more gradual intensity gradients across the field, with fewer sharp column/row artifacts. This smoother distribution suggests lower fixed-pattern spatial variation or better intrinsic uniformity. Histograms show tighter clustering of pixel values, especially at medium integration times, pointing to more consistent gain and offset across the sensor. However, some residual non-linearities may be inferred from broader distributions at longer integration times.

4.3 Temporal non-uniformity VOC

This sub-section analyses frame-to-frame variation over time at the pixel level using:

- Time series plots of selected pixels (Fig. 7).
- Pixel-wise standard deviation heatmaps (Fig. 8).
- Histograms of pixel variation across frames (Fig. 9).

4.3.1 Pixel intensity over time (100 frames, 5x pixels)

In Fig. 7(a)-(b) the temporal pixel plots for 5 representative pixels for 1ms and 16ms integration times are shown ranging from high to low temporal variation. Each trace shows pixel value across 100 frames.

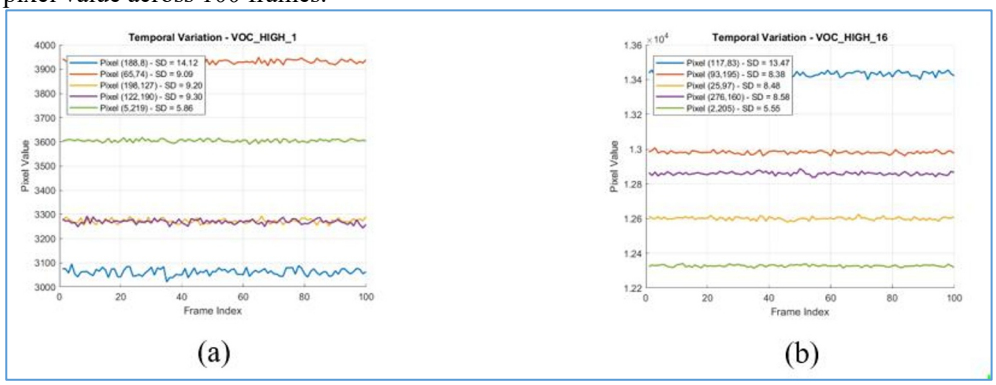

Fig. 7. Temporal pixel plots at (a) 1ms and (b) 16ms integration times.

4.3.2 Pixel temporal variation heatmaps

In Fig. 8(a)-(b) heatmaps of per-pixel standard deviation computed over 100 frames are shown. Higher values indicate areas of increased temporal instability.

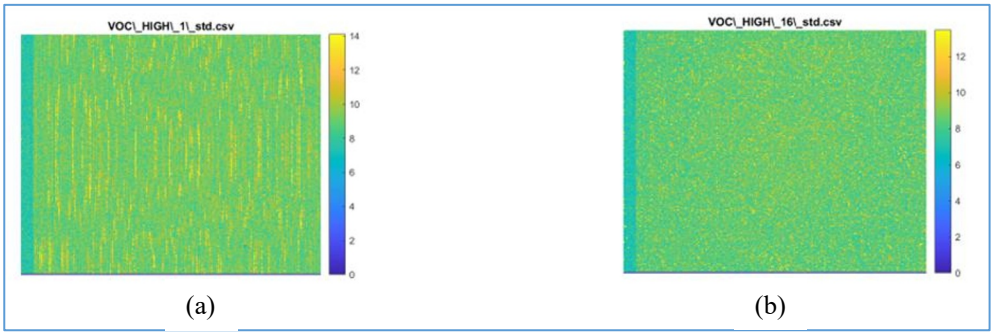

Fig. 8. Per-pixel standard deviation for (a) 1ms and 16ms integration times.

4.3.3 Pixel intensity histogram (100 frames, 5x pixels)

Fig. 9(a)-(b) show the histograms of pixel standard deviation.

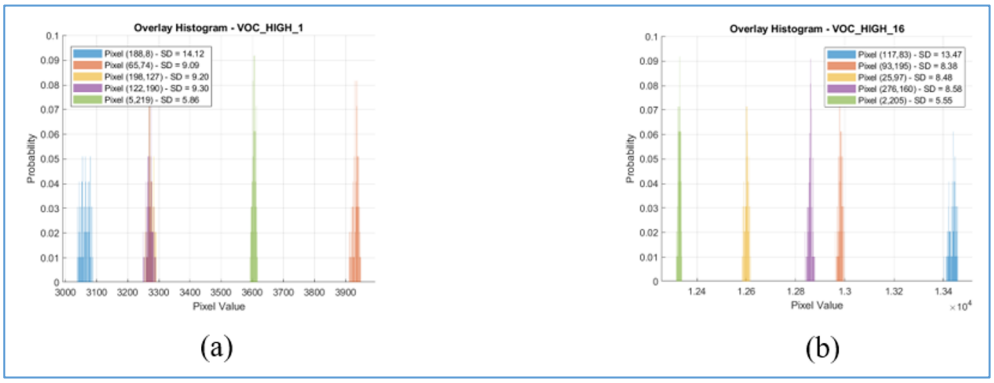

Fig. 9. Pixel intensity for 100 frames at (a) 1ms and (b) 16ms integration times.

4.3.4 Discussion - temporal non-uniformity VOC

Temporal pixel plots for the VOC camera indicate considerable variation across selected pixels (Fig. 7). High-standard-deviation pixels show pronounced noise over the 100 frames, while more stable pixels remain relatively constant. The standard deviation heatmaps (Fig. 8) illustrate spatial variability in temporal noise — some regions are consistently noisier, which could point to issues in specific pixel blocks or column amplifiers. Histograms of per-pixel temporal standard deviation (Fig. 9) show a roughly normal distribution.

4.4 Temporal non-uniformity SF6

This sub-section analyses frame-to-frame variation over time at the pixel level using:

- Time series plots of selected pixels (Fig. 10)
- Pixel-wise standard deviation heatmaps (Fig. 11)
- Histograms of pixel variation across frames (Fig. 12)

4.4.1 Pixel intensity over time (100 frames, 5x pixels)

Fig. 10(a)-(b) show temporal pixel plots for selected pixels in SF6 detector, showing frame-to-frame variation.

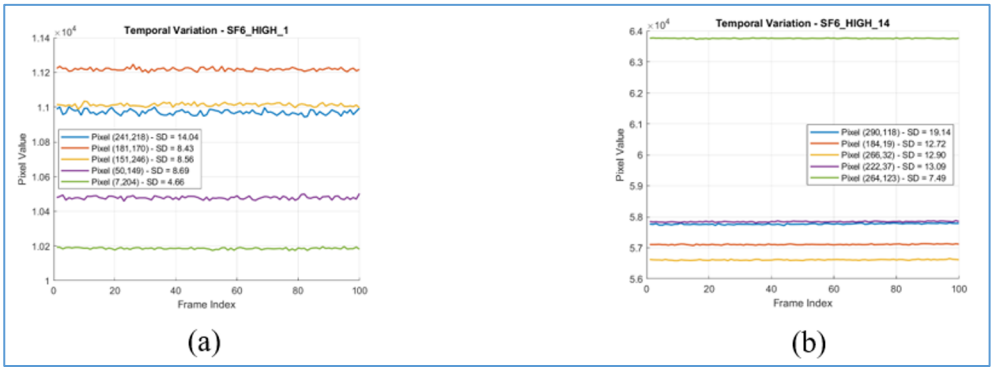

Fig. 10. Temporal variation pixel plots at (a) 1ms and (b) 16ms integration times.

4.4.2 Pixel temporal variation heatmaps

In Fig. 11(a)-(b) the standard deviation heatmaps for the SF6 sensor is shown.

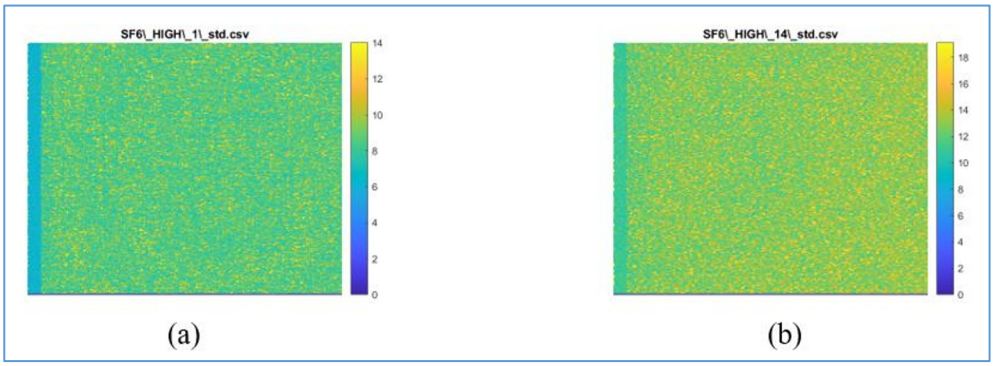

Fig. 11. Per-pixel standard deviation for (a) 1ms and (b) 16ms integration times.

4.4.3 Pixel intensity histogram (100 frames, 5x pixels)

Fig. 12(a)-(b) shows the histograms of temporal deviation across SF6 detector pixels.

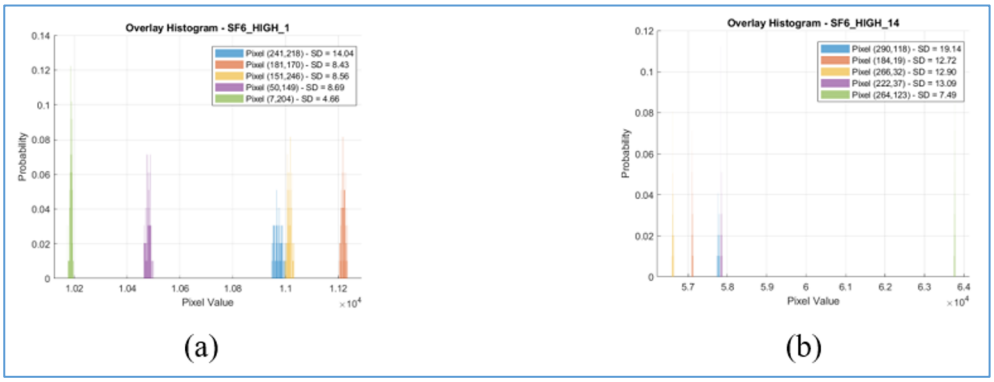

Fig. 12. Pixel intensity for100 frames at (a) 1ms and (b) 16ms integration times.

4.4.4 Discussion - temporal non-uniformity SF6

Similar to VOC, the SF6 temporal pixel plots indicate considerable variation across selected pixels (Fig. 10). The standard deviation heatmaps (Fig. 11) illustrate spatial variability in temporal noise. The SF6 camera shows less spatially structured temporal noise than the VOC camera. Histograms of per-pixel temporal standard deviation show a roughly normal distribution (Fig. 12).

4.5 Gain and offset map VOC

The gain and offset maps for the VOC detector are 1ms and 16ms integration times are presented in the following subsections.

4.5.1 Gain and offset heatmaps

Fig. 13 and Fig. 14 show the gain and offset maps for VOC detector. Spatial variability is evident, with regions of higher and lower responsivity.

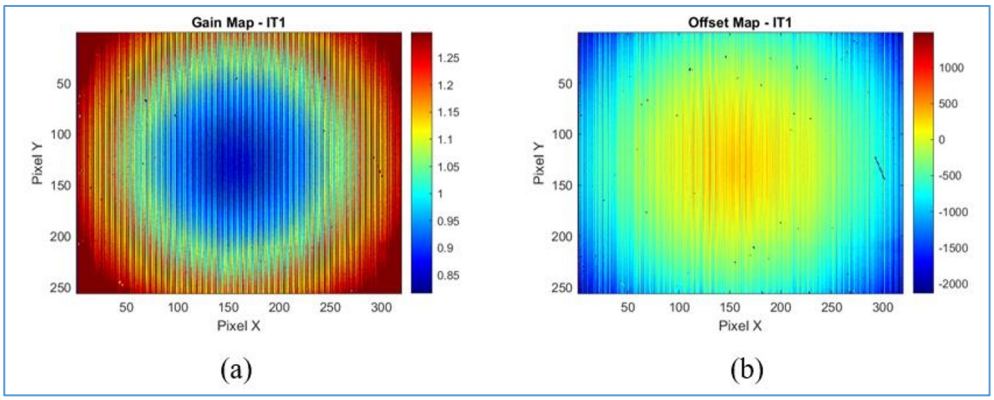

Fig. 13. (a) Gain and (b) offset maps for VOC detector at 1ms integration time.

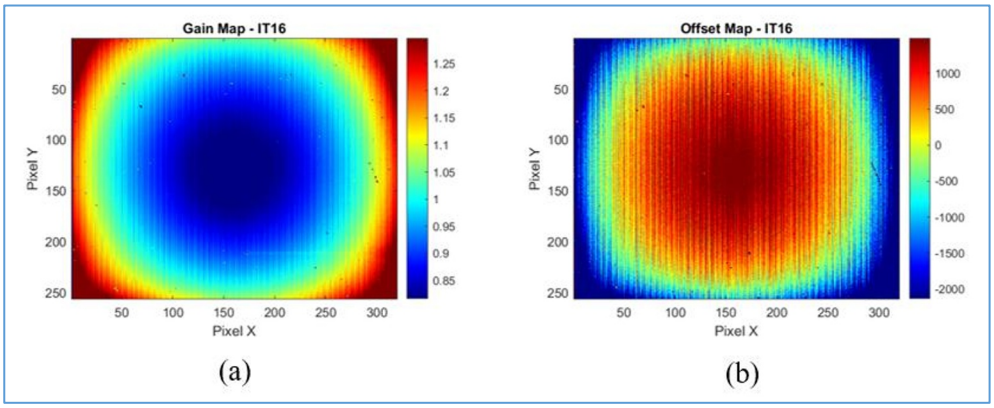

Fig. 14. (a) Gain and (b) offset maps for VOC detector at 16ms integration time.

4.5.2 Discussion – gain and offset map VOC

The gain and offset maps for the VOC detector (Fig. 13 - Fig. 14), calculated from the two-point calibration frames, exhibit significant spatial variability. The gain map reveals areas of both higher and lower responsivity, indicating mismatches in pixel amplification across the sensor. The offset map similarly shows patterns suggestive of additive readout noise or baseline mismatches. Visual inspection shows these maps are not flat, underscoring the importance of effective NUC techniques for this sensor.

4.6 Gain and offset map SF6

The gain and offset maps for the SF6 detector are 1ms and 16ms integration times are presented in the following subsections.

4.6.1 Gain and offset heatmaps

Fig. 15 and Fig. 16 show the gain and offset maps for SF6 detector. More uniform patterns imply better factory matching or pixel-level uniformity.

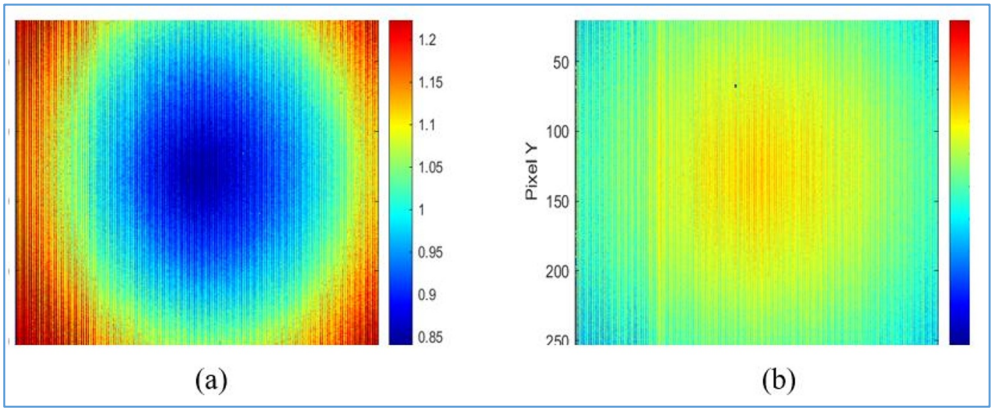

Fig. 15. (a) Gain and (b) offset maps for SF6 detector at 1ms integration time.

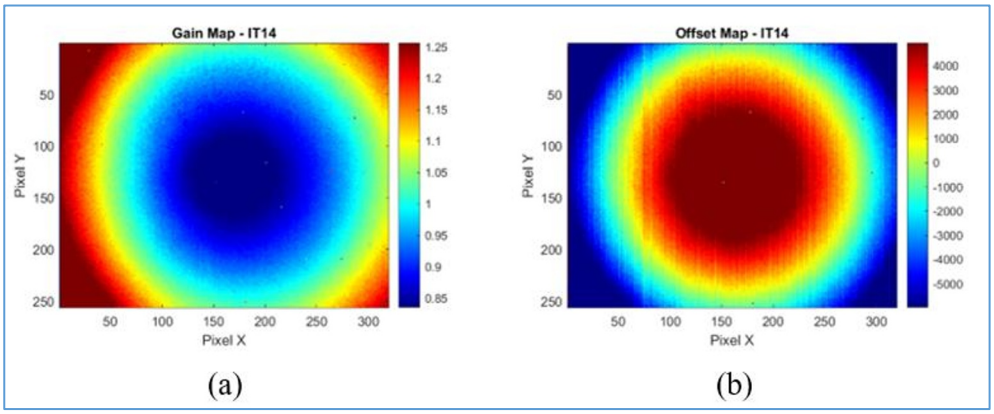

Fig. 16. (a) Gain and (b) offset maps for SF6 detector at 14ms integration time.

4.6.2 Discussion – gain and offset map SF6

The SF6 gain and offset maps (Fig. 15 - Fig. 16) appear more uniform than those of the VOC detector. The gain variation is less pronounced, suggesting more consistent pixel responsivity. Offset maps are similarly smoother, with fewer large deviations, reflecting better calibration or intrinsic detector uniformity. These characteristics likely contribute to the SF6 sensor's lower residual and temporal noise. The results support the notion that the SF6 FPA is more consistent across pixels in both multiplicative (gain) and additive (offset) terms.

4.7 Residual non-uniformity VOC

This sub-section shows the difference between corrected frames and the ideal frame.

4.7.1 Residual non-uniformity

This sub-section (Fig. 17 - Fig. 19) presents a summary metric, the median absolute residual per frame, showing how much each frame deviates from the ideal.

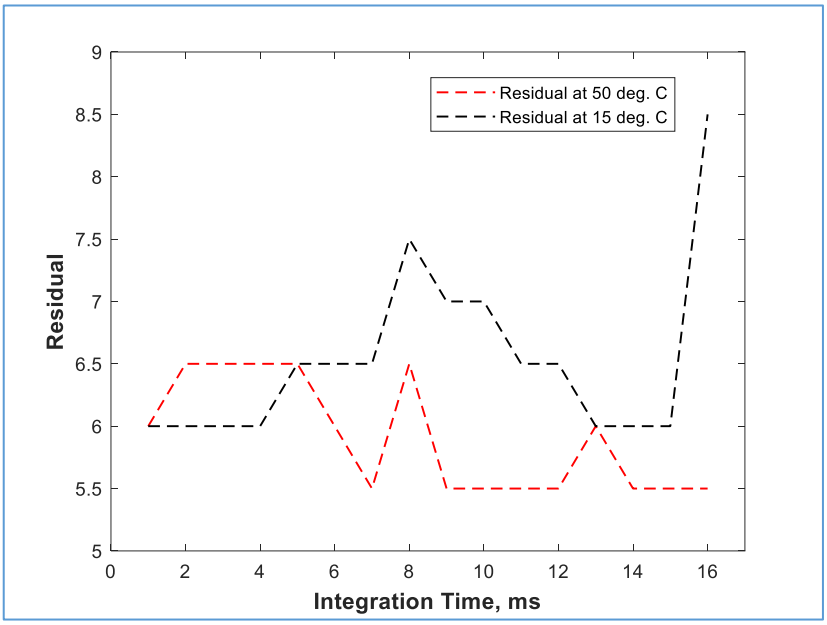

Fig. 17. Median absolute residuals per integration time for high and low temperature scenes for the VOC detector.

4.7.2 Residual non-uniformity spatial distribution heatmaps

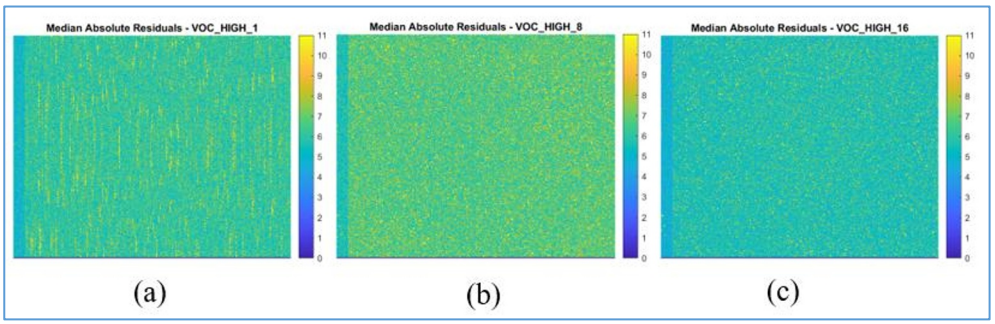

Fig. 18. Heatmaps for VOC detector at (a) 1ms, (b) 8ms and (c) 16ms integration times.

4.7.3 Residual non-uniformity median frame histogram

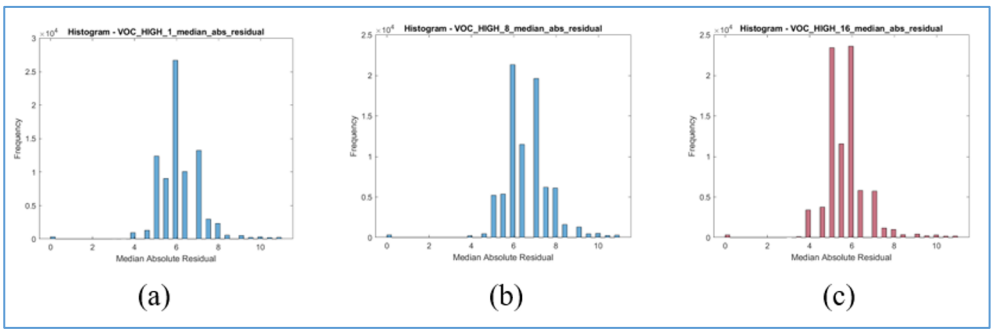

Fig. 19. Histogram for VOC detector at (a) 1ms, (b) 8ms and (c) 16ms integration times.

4.7.4 Discussion – residual non-uniformity VOC

Despite NUC application, residual maps for the VOC detector (Fig. 17 – Fig. 19) demonstrate remaining non-uniformities. The residual heatmaps reveal structures aligned with the original fixed-pattern noise, albeit reduced in magnitude. Residuals are higher at shorter integration times, likely due to lower signal levels, which amplify relative errors in gain and offset correction. Histograms of residual pixel values show non-zero-centred distributions, indicating over- or under-compensation in the correction process for some pixels. Overall, this suggests that while the two-point NUC reduces non-uniformity, further correction (e.g., non-linearity compensation or higher-order correction) may be needed.

4.8 Residual non-uniformity SF6

This sub-section shows the difference between corrected frames and the ideal frame for the SF6 detector.

4.8.1 Residual non-uniformity

This sub-section (Fig. 20 - Fig. 22) presents a summary metric, the median absolute residual per frame, showing how much each frame deviates from the ideal.

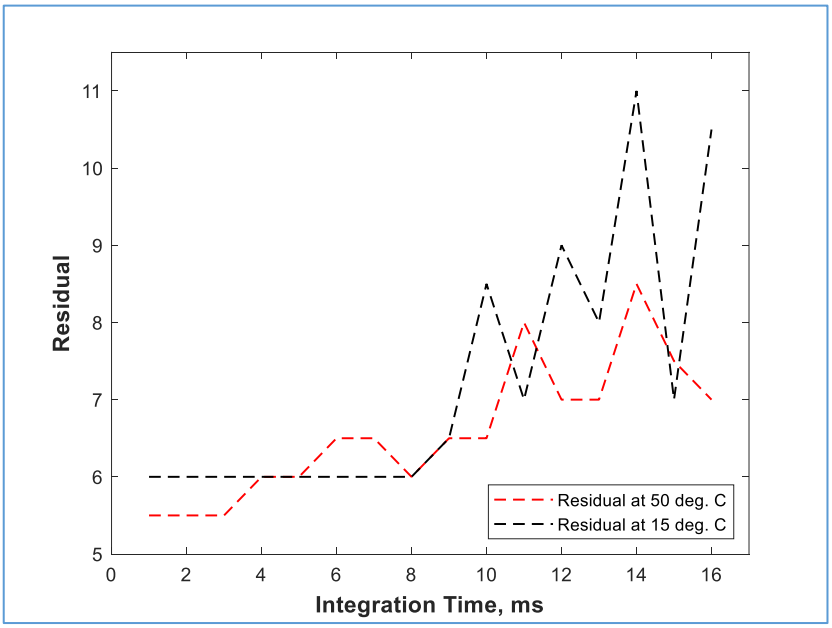

Fig. 20. Median absolute residuals per integration time for high and low temperature scenes for the SF6 detector.

4.8.2 Residual non-uniformity spatial distribution heatmaps

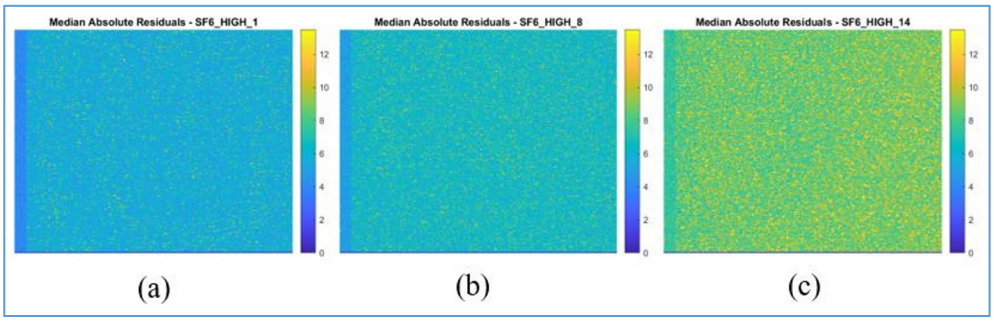

Fig. 21. Heatmaps for SF6 detector at (a) 1ms, (b) 8ms and (c) 14ms integration times.

4.8.3 Residual non-uniformity median frame histogram

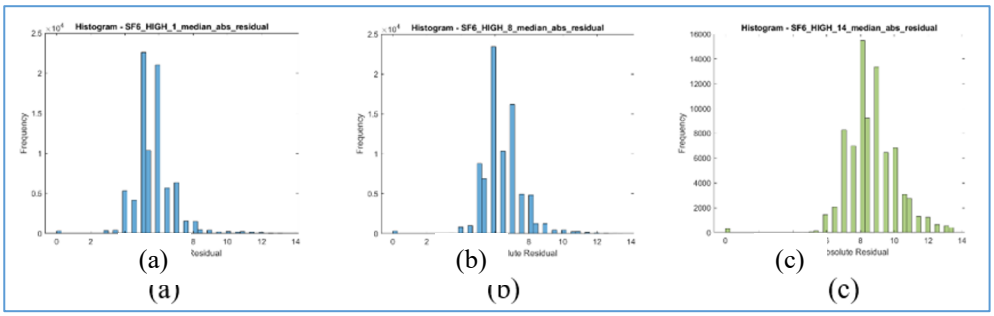

Fig. 22. Histogram for SF6 detector at (a) 1ms, (b) 8ms and (c) 16ms integration times.

4.8.4 Discussion – residual non-uniformity SF6

For the SF6 detector (Fig. 20 – Fig. 22), residual maps post-NUC are marginally better. Most residuals are centred near zero, and structured noise is minimal. This suggests that the two-point NUC was effective, yet not perfect.

5 Conclusion

This study evaluated the spatial and temporal non-uniformity characteristics of two infrared sensors, VOC and SF6, using a systematic approach combining visualizations, statistical measures, and pixel-level analysis. The characterization included analysis of median frames, pixel standard deviation over time, gain and offset maps, and post-correction residuals across 16 integration times. Residual visualizations confirmed that both SF6 and VOC cameras responded well to NUC (non-uniformity correction), producing low residual values and less remaining structure across integration times. However, the VOC sensor exhibited higher framewise variation, more prominent structured noise. Although the current two-point NUC correction yielded visible improvements, several opportunities exist for further enhancement:

Hot pixel detection and suppression: Identifying and masking or replacing outlier pixels may improve the overall correction quality and downstream image quality.

Temporal drift and stability monitoring: Extending the analysis to evaluate correction stability over time, under thermal drift or operating stress, could validate long-term performance.

References

1. R. Ivanov et al, III-V based infrared detectors are imposing new standards, Proc. SPIE, **114070**, 114070Q (2020). https://doi.org/10.1117/12.2558736
2. I. Ribet-Mohamed et al, Residual fixed pattern noise and random telegraph signal noise of a MWIR T2SL focal plane array, in Proc. SPIE **11002**, 110020E (2019). https://doi.org/10.1117/12.2520211
3. H. Martijn et al, QWIPs at IRnova, a status update, in Proc. SPIE **9819**, 981918 (2016). https://doi.org/10.1117/12.2228348
4. Xingang Mou et al, Background modeling for adaptive nonuniformity correction in IRFPA, in 2010 International Conference on Optics, Photonics and Energy Engineering, Wuhan, China May 10-11 (2010), 84
5. P. Goyal, Studying the performance parameters on real infrared image/data and evaluation by application of the NUC algorithm, in 2010 International Conference on Industrial Electronics, Control and Robotics, Rourkela, India, December 28-29 (2010), 65
6. Y. Cao, M. Y. Yang and C. Tisse, Effective strip noise removal for low-textured infrared images based on 1-D guided filtering, IEEE Trans. on Circuits and Systems for Video Technology, **26**, 2176, (2016)
7. L. Mingqing, Y. Wang and H. Sun, Single-frame infrared image non-uniformity correction based on wavelet domain noise separation, Sensors, **23**, 8424, (2023)
8. M. R. Lovejoy and M. A. Wickert, Testing an improved gain equalization non-uniformity correction algorithm, in 2018 IEEE Aerospace Conference, Big Sky, MT, USA, March 3-10 (2018)
9. M. Rozkovec and J. Cech, Polynomial based NUC implemented on FPGA, in 2016 Euromicro Conference on Digital System Design, DSD, Limassol, Cyprus, August 1 (2016)
10. N. Kumar, M. Massey and N. Kandpal, Least square regression based non-uniformity correction for infra-red focal plane arrays, in 2019 International Conference on Range Technology, ICORT, Balasore, India, February (2019)
11. G. Wen et al, Advances in Natural Computation, Fuzzy Systems and Knowledge Discovery, (Springer Nature, Switzerland AG 2020)
12. A.B.G., Operating the IRnova320ER IDCA series, (IRnova A.B., Kista, Sweden)
13. M. Chirindo, E. Cox and K. Duness, An optical gas imaging technique based on strobed illumination, in 2024 RAPDASA-RobMech-PRASA-AMI Conference, Gqeberha, South Africa, October 28-31 (2024)